Supporting Information

Near-infrared responsive gold nanorods for highly sensitive colorimetric and photothermal lateral flow immuno-detection of SARS-CoV-2

Xiaohui Liu[a#], Jingwen Li[a#], Kun Wang[a], Xiang Li[a], Shenming Wang[a], Gengchen Guo[a], Qiaowen Zheng[a], Maosheng Zhang[b*], Jingbin Zeng[a,*]

[a] *College of Chemistry and Chemical Engineering and State Key Laboratory of heavy oil processing, China University of Petroleum (East China), Qingdao, 266580, China. Email: zengjb@upc.edu.cn*

[b] *College of Chemistry and Environment, Fujian Provincial Key Laboratory of Modern Analytical Science and Separation Technology, Minnan Normal University, Zhangzhou 363000, China.*

[#]*These authors contributed equally to this work.*

1. Experiment Section

Measurement of photothermal conversion efficiency To assess the photothermal effects of the four GNRs, the photothermal conversion efficiency was measured and calculated. Temperature changes were monitored by taking 1 mL of water and four GNRs solutions with 808 nm laser irradiation at a power density of 1.69 W/cm^2. After the temperature was flat and cooled to room temperature, the temperature of the process was recorded with an infrared thermal imager.

Calculate the photothermal conversion efficiency (η) according to the reported method[1]:

$$\eta = \frac{hs(T_{max} - T_{sur}) - hs(T_{max(water)} - T_{sur(water)})}{I(1 - 10^{-A_{808}})}$$

h is the heat transfer coefficient; s is the surface area of the container. I is the laser power and A is the absorbance at 808 nm. $T_{max(water)}$ is the maximum temperature of water. $T_{sur(water)}$ is the environmental temperature of water.

$$hs = \frac{mc_{water}}{\tau_s}$$

m is the mass of the water, c is the specific heat capacity of the water (c_{water} = 4.2 J/(g•°C)), and τ_s is the associated time constant.

$$t = -\tau_s ln(\theta)$$

θ is the driving force temperature and dimensionless.

$$\theta = \frac{T - T_{sur}}{T_{max} - T_{sur}}$$

T_{max} and T_{Sur} are the maximum temperature and the environmental temperature of solutions, respectively.

2. Supporting Figures

Characterization of GNRs and GNRs-Ab

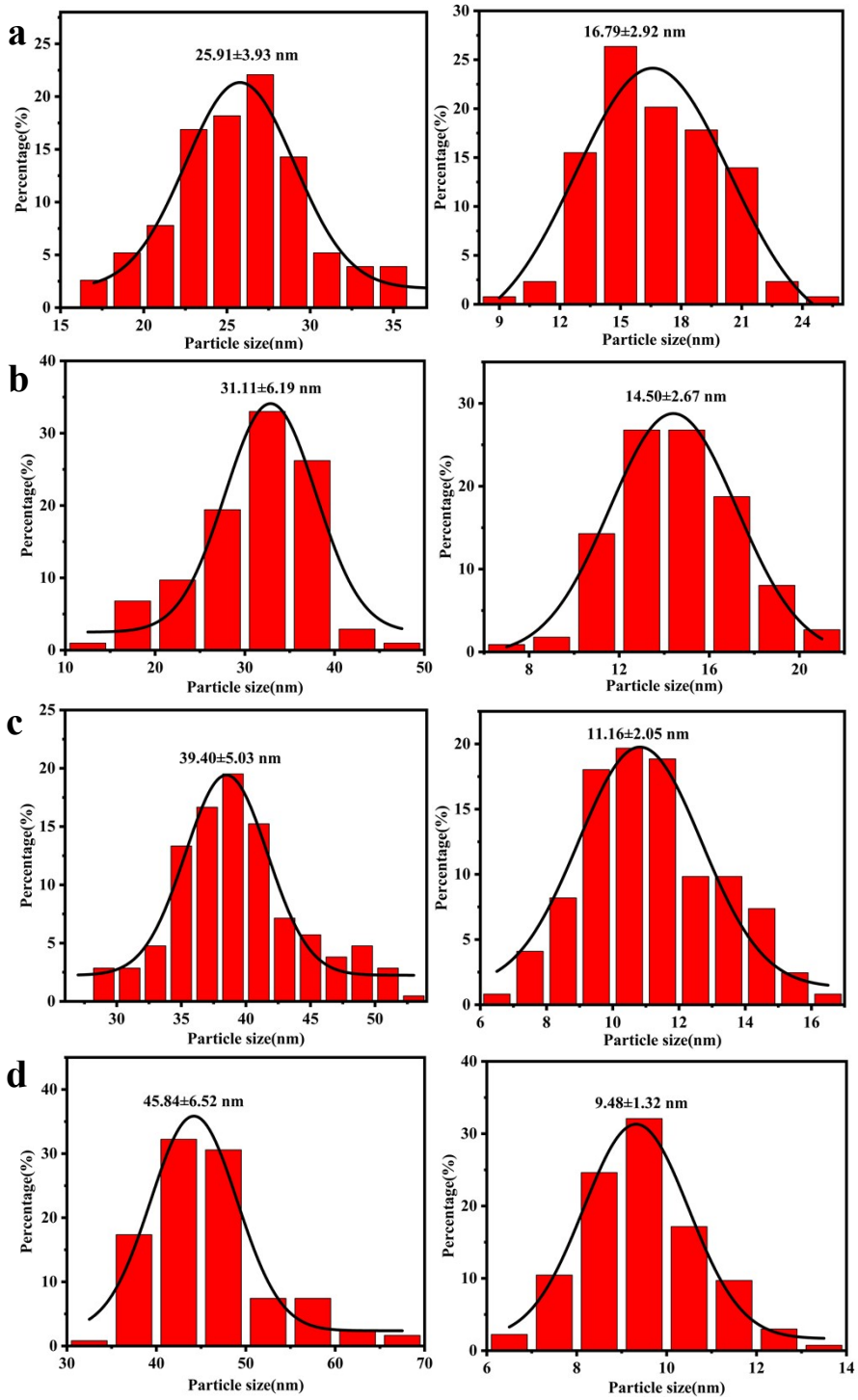

Fig. S1 Particle size distribution of GNRs with different aspect ratios (a) 1.55 (b) 2.28 (c) 3.56 (4) 4.74 Radial particle size distribution is shown on the left and transverse particle distribution on the right

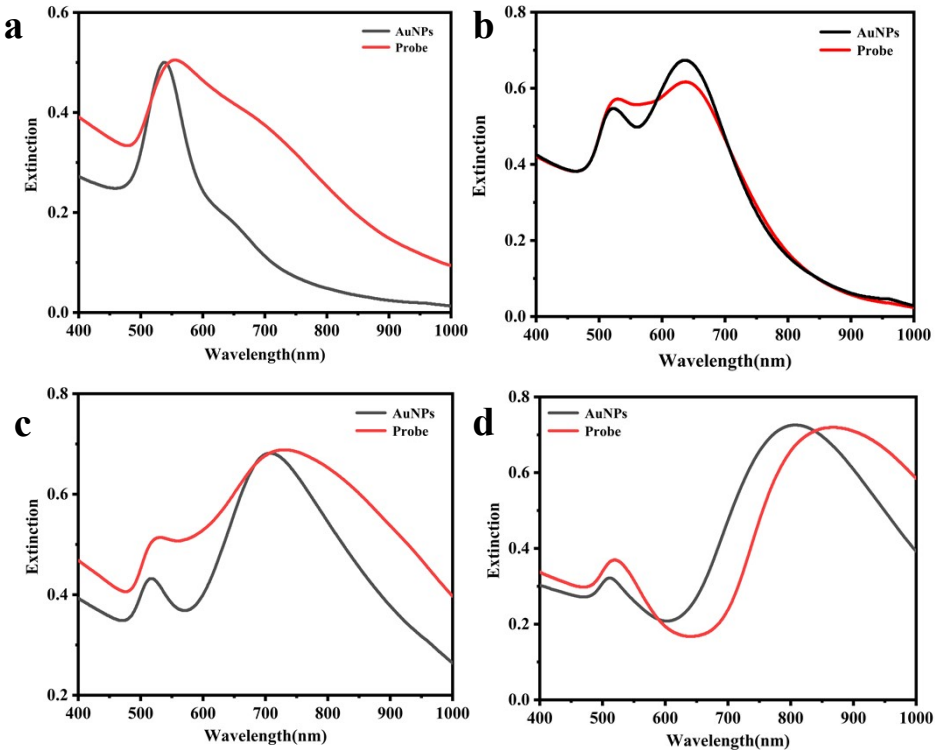

Fig. S2 UV-visible absorption spectrum of different LSPR absorption wavelength GNRs and GNRs-Ab (a) 538 nm (b) 632 nm (c) 726 nm (d) 808 nm

Optimization of the detection conditions

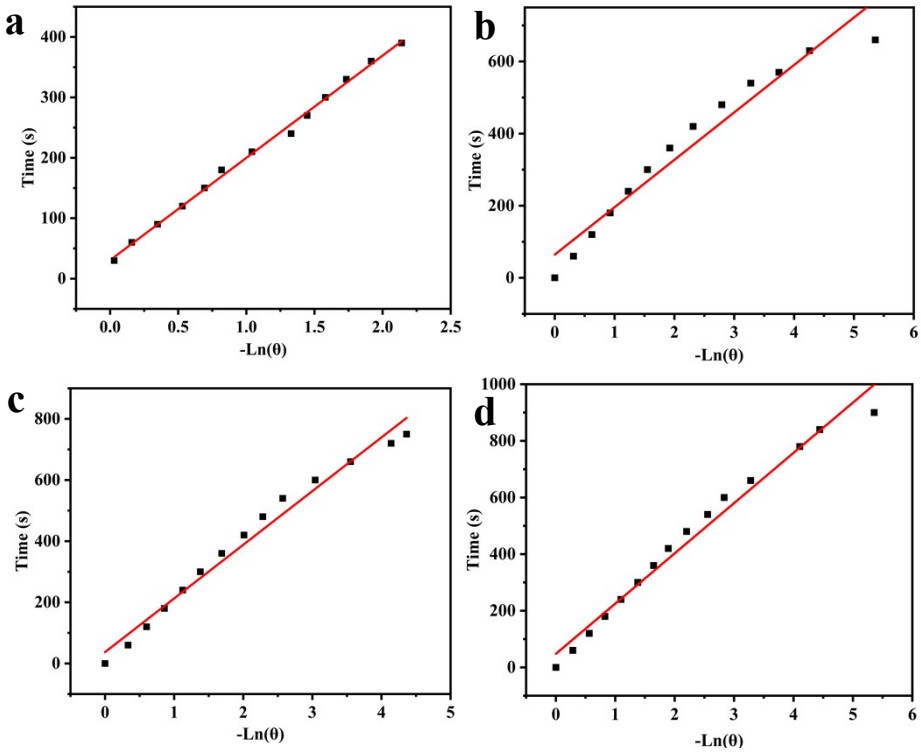

Fig. S3 Heat transfer time constants for GNRs with four different wavelengths (a) 538 nm (b) 632 nm (c) 726 nm (d) 808 nm

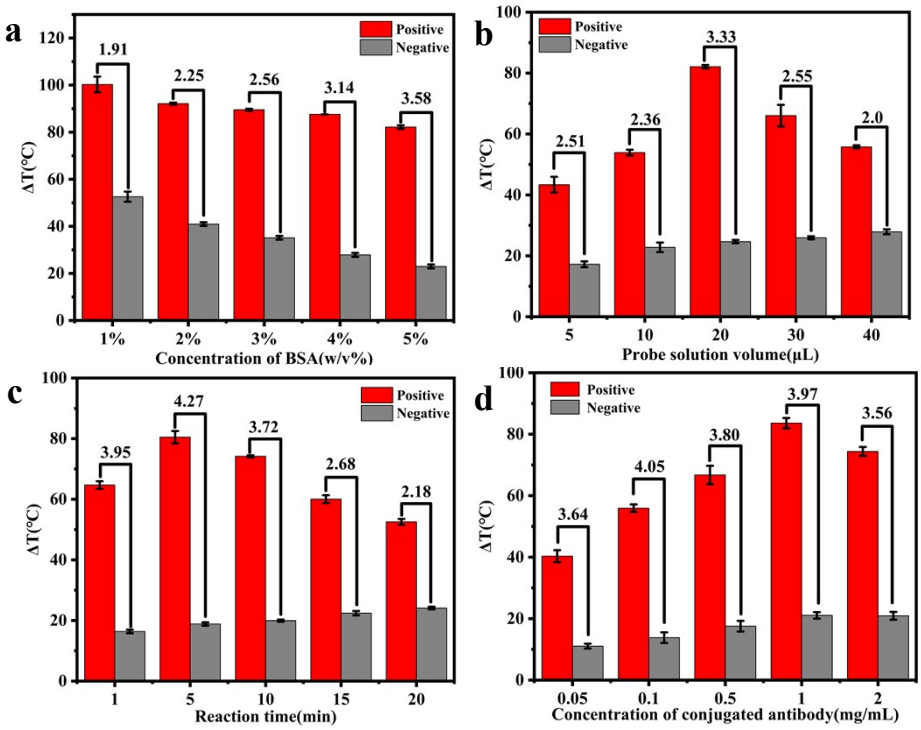

Fig. S4 Optimization of the photothermal detection conditions (a) Histograms of the photothermal detection signals after sealing of different concentrations of BSA (b) Histograms of photothermal detection signals for different probe amounts (c) Histograms of the photothermal detection signals for different incubation time (d) Histograms of photothermal detection for different amounts of conjugated antibodies. Error bars were calculated from three sets of experiments

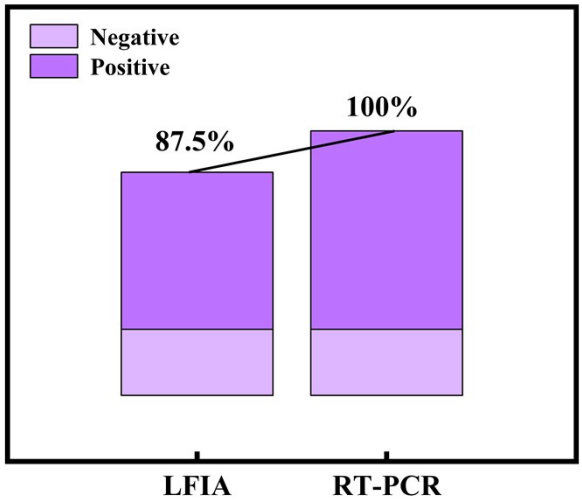

Fig. S5 Comparison of LFIA strips and RT-PCR for real samples

3. Supporting Tables

Characterization of GNRs

Table S1 Transverse and longitudinal absorption peaks of GNRs synthesized with different amounts of silver nitrate

$V(AgNO_3)$ /μL	transverse SPR absorption peaks	longitudinal SPR absorption peaks
15	538 nm	-
30	534 nm	632 nm
60	520 nm	726 nm
80	520 nm	808 nm

Calculation of detection limits

Table S2 Data from the photothermal measurements for the calibration curve of Fig.4b

△T (°C) \ Concentration (μg/mL)	0.4	0.04	0.004	0.002	0.0004	0.0002	0
1	75.536	50.324	35.624	27.424	21.424	15.824	6.824
2	75.824	52.844	38.624	25.124	21.924	15.624	7.425
3	74.014	56.124	34.224	26.324	18.524	15.224	5.324
Mean	75.124	53.097	36.157	26.290	20.624	15.557	6.524
SD	0.972	2.908	2.248	1.150	1.836	0.305	1.082

Real sample detection

Table S3 Detailed detection results of the actual samples

Sample number	LFIA		Mingde Ct value	
	C-line	T-line	ORF1ab	N

P01	+	+	27.71	27.37
P02	+	++	23.6	23.15
P03	+	+	20.82	20.29
P04	+	-	27.7	26.41
P05	+	++	21.73	20.73
P06	+	++	17.69	17.74
P07	+	-	25.53	24.46
P08	+	-	27.49	27.33
P09	+	+	24.4	24.8
P10	+	┼	18.96	18.48
P11	+	++	21.64	20.71
P12	+	-	21.68	21.59
P13	+	+	27.87	27.45
P14	+	++	20.62	21.33
P15	+	-	24.85	24.34
P16	+	+	21.41	20.56
P17	+	+	20.91	20.57
P18	+	++	23.37	23.5
P19	+	++	20.43	20.37
P20	+	+	19.66	19.84
P21	+	+	23.51	23.3
P22	+	+	27.39	27.21
P23	+	+	22.64	22.34

P24	+	++	21.82	21.89
P25	+	++	21.89	21.9
P26	+	+	22.86	21.95
P27	+	++	19.7	18.77
P28	+	++	21.31	20.69
P29	+	+	22.74	22.74
P30	+	+	18.99	19.14
P31	+	+	23.17	22.77
P32	+	+	26.93	25.71
N01	+	-	-	-
N02	+	-	-	-
N03	+	-	-	-
N04	+	-	-	-
N05	+	-	-	-
N06	+	-	-	-
N07	+	-	-	-
N08	+	-	-	-

The samples tested were samples of uninactivated COVID-19 cases. Sample number P was positive and N was negative. “+” means that the stripe shows color; “++” means that the stripe shows a darker color.; “-” indicates that the stripe does not show color. The Ct value is the basis for determining the infection. The Ct value less than 35 means a positive test result.

Table S4 Summary of the analytical performances of the detection of SARS-CoV-2 N protein with different methods

Method	Label	Signal	LOD	Ref
Microfluidic ELISA	TMB enzyme	Color	0.013 ng/mL	[2]
Fluid array	MagPlex microspheres	Fluorescence	0.050 ng/mL	[3]
LFIA	Au@4-MBA@Ag	Raman	0.03 ng/mL	[4]
LFIA	AIEgens	Fluorescence	7.2 ng/mL	[5]
LFIA	CNB	Color	＞ 1 ng/mL	[6]
LFIA	Latex beads	Color	0.65 ng/mL	[7]
LFIA	Au NPs	Color	40 ng/mL	Previous work [8]
LFIA	Au NRs	Photothermal	0.096 ng/mL	This work

Reference

[1] Xi, D.M., Xiao, M., Cao, J.F., Zhao, L.Y., Xu, N., Long, S., Fan J.L., Shao, K., Sun, W., Yan, X.H., Peng, X.J., 2020. Adv. Mater. 32(11), e1907855.

[2] Bhuiyan, N.H., Uddin, M.J., Lee, J., Hong, J.H., Shim, J.S., 2022. Advanced Materials Technologies 7(9), 2101690.

[3] Anderson, G.P., Liu, J.L., Esparza, T.J., Voelker, B.T., Hofmann, E.R., Goldman, E.R., 2021. Anal. Chem. 93(19), 7283-7291.

[4] Lai, S., Liu, Y., Fang, S., Wu, Q., Fan, M., Lin, D., Lin, J., Feng, S., 2023. J. Biophotonics. 16, e202300004.

[5] Zhang, G.Q., Gao, Z., Zhang, J., Ou, H., Gao, H., Kwok, R.T.K., Ding, D., Tang, B.Z., 2022. Cell Rep Phys Sci 3(2), 100740.

[6] Kim, H.Y., Lee, J.H., Kim, M.J., Park, S.C., Choi, M., Lee, W., Ku, K.B., Kim, B.T., Changkyun Park, E., Kim, H.G., Kim, S.I., 2021. Biosens. Bioelectron. 175, 112868.

[7] Grant, B.D., Anderson, C.E., Williford, J.R., Alonzo, L.F., Glukhova, V.A., Boyle, D.S., Weigl, B.H., Nichols, K.P., 2020. Anal. Chem. 92(16), 11305-11309.

[8] Li, X., Yu, D., Li, H.W., Sun, R.C., Zhang, Z.R., Zhao, T.Y., Guo, G.C., Zeng, J.B., Wen, C.Y., 2023. Biosens. Bioelectron. 241, 115688.